BIBECHANA
Vol. 22, No. 3, December 2025, 258-265

ISSN 2091-0762 (Print), 2382-5340 (Online)
Journal homepage: http://nepjol.info/index.php/BIBECHANA
Publisher:Dept. of Phys., Mahendra Morang A. M. Campus (Tribhuvan University)Biratnagar

A DFT based study of structural, electrical and vibrational properties of LiFeAs – A pnictide superconductor

Aditya M. Vora

Department of Physics, University School of Sciences, Gujarat University, Navrangpura, Ahmedabad 380 009, Gujarat, India
*Corresponding author. Email: voraam@gmail.com

Abstract

By the uses of ultrasoft pseudopotential and the generalized gradient approximation (GGA), we have looked at the structural, electrical and vibrational characteristics of the LiFeAs pnictide superconductor in the present work. There is a strong correlation between phonons and superconductivity, which is the major root of the superconductivity of iron pnictide superconductors. The superconducting characteristics of materials can be predicted using phonon properties. According to studies using density functional theory (DFT), LiFeAs exhibits its metallic nature in the overlaying bands close to the Fermi level. The dynamical stability is supported by positive frequencies in the phonon dispersion curves.

Keywords
Density functional theory (DFT), Generalized gradient approximation (GGA), ultrasoft pseudopotential, Iron pnictide superconductors, Phonon dispersion curves.

Article information
Manuscript received: April 18, 2025; Revised: August 13, 2025; Accepted: August 16, 2025
DOI https://doi.org/10.3126/bibechana.v22i3.77717

1 Introduction

The discovery of superconductivity in iron-based layered compounds by Kamihara et al. [1] sparked a fierce search for new pnictide and chalcogenide superconductors. In early reviews and theoretical overviews, these materials were classified as a distinct class based on FeAs or FeSe layers, which are critical to superconductivity [2–10]. LiFeAs, a 111-type pnictide, is unique among them due to its intrinsic superconductivity without chemical doping [11, 12]. Without the added complications of disorder, this material offers a clean platform for examining the underlying mechanisms.

Extensive experimental and theoretical studies of the structural and magnetic properties of iron pnictides have revealed strong electronic correlations [13], unusual magnetic interactions [14], and the possible coexistence or competition between magnetism and superconductivity [14–21]. While spin fluctuations are often cited as a possible glue for pairing [22], other options include electron-phonon interaction or synergistic effects. However, optical and penetration-depth measurements further emphasize the complex interplay between the carrier dynamics and superconducting gap struc-

ture [16,23].

LiFeAs has attracted a lot of attention within this broader family due to its unusual lack of the Fermi surface nesting [24], which calls into the question of conventional spin-density-wave-based pairing models. Comparative first-principles simulations with related compounds such as LiFeP [25,26] and high-pressure experiments [27] have shown that subtle changes in the pnictogen height and lattice properties have a substantial effect on the density of states at the Fermi level and, thus, the superconducting capabilities. These findings have demonstrated how important it is to understand such materials through accurate electronic structure calculations and structural optimization, which density functional theory (DFT) provides.

Despite these strides, gaps remain. Phonon dispersion data are also sparse relative to electronic structure data, and measured lattice constants for LiFeAs vary between experiments as well as compared to computational studies. The respective roles of spin fluctuations and lattice vibrations in superconductivity in LiFeAs remain controversial. Also, some phonon studies indicate insufficient electron–phonon coupling to account for the observed Tc [8,28], whereas others point to possible cooperative effects in the examined materails. And yet, there still remains no integrated study of structural, electronic, and vibrational properties within the same computational setting. This study conducts a systematic DFT analysis of LiFeAs, focusing on its structure, electronic band structure, and vibrational spectra in order to fill in the gaps. By integrating these factors, the study seeks to elucidate the fundamental properties of the material that influence its superconductivity and to establish computational models that can guide later experimental and theoretical investigations.

LiFeAs crystallizes in the tetragonal P4/nmm space group and has a Matlockite structure. Li^{1+} forms distorted $LiAs_5$ trigonal bipyramids when it is bonded to five equivalent As_3 atoms. These trigonal bipyramids share corners with 12 equivalent $FeAs_4$ tetrahedra, edges with four equivalent $FeAs_4$ tetrahedra, and edges with eight equivalent $LiAs_5$ trigonal bipyramids. All Li-As bonds have a length of 2.67Å. Fe^{2+} forms distorted $FeAs_4$ tetrahedra by bonding with four equivalent As_3 atoms, which share corners with four equivalent $FeAs_4$ tetrahedra, edges with four equivalent $LiAs_5$ trigonal bipyramids, and corners with twelve equivalent $LiAs_5$ trigonal bipyramids. The average Fe-As bond length is 2.47Å. As_3 is coupled to five equivalent Li^{1+} and four equivalent Fe^{2+} atoms in a nine-coordinate geometry [29].

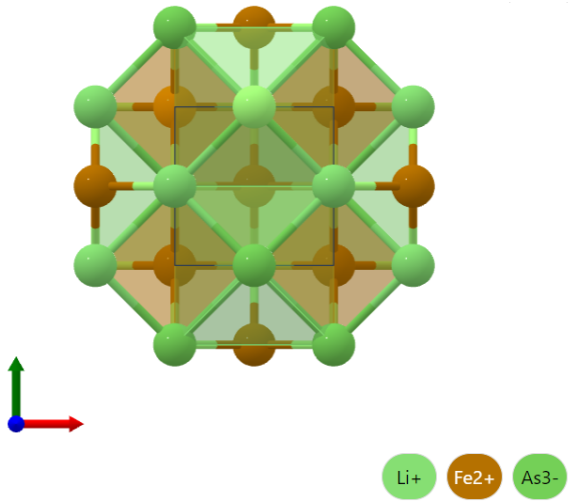

Figure 1: Crystal structures of LiFeAs.

Currently, it is observed that simulations based on Density Functional Theory (DFT) [30–39] are more accurate when examining the physical characteristics of different materials. Studying the structural, electrical, vibrational, and superconducting properties of LiFeAs iron pnictide superconductors under DFT environment is the focus of the current work, which is motivated by the significance of the superconductivity phenomenon and its applications in many fields.

2 Theory

Using the Quantum Espresso (QE) code [40], a DFT based computations are carried out to investigate the structural, electrical, vibrational, and superconducting properties of LiFeAs. Because it favours density inhomogeneity, the Generalized Gradient Approximation (GGA) with Perdew-Burke-Einzerhof (PBE) [41] functional is used to analyze the exchange correlation effects.

The plane waves with a charge density cutoff of 80 Ry and a kinetic energy cutoff of 20 Ry are considered here. The 4x4x4 k-point mesh is used to highlight integration over the Brillouin zone. In this work, the ultrasoft pseudopotentials [42] of three distinct elements—Li, Fe, and As are employed.

Since convergence tests revealed insignificant energy changes outside of this mesh, a 4×4×4 Monkhorst–Pack k-point mesh was used for geometry optimizations in this work to lower computational cost while maintaining accurate forces and stresses. A denser 6×6×6 mesh was used for the final electronic structure and DOS calculations in order to guarantee precise Brillouin zone integration and fine resolution close to the Fermi level.

3 Results and Discussion

Figure 1 displays the optimization curves for the kinetic energy cutoff (Ecut), k-grid, and the cell parameter ratio (c/a) for LiFeAs. Using the variable cell relaxation (vc-relax) approach, the atomic location of said material and the lattice constants were first optimized. To confirm the findings, ration of the lattice parameters (c/a) was then adjusted. The relaxed parameters were achieved by applying the GGA technique with ultrasoft pseudopotentials, as implemented in QE. Table 1 presents a comparison among the computed optimized lattice parameter results and the available experimental outcomes [12]. In the present computation, the optimized lattice parameter is obtained a=3.790A, which found in good agreement with the available experimental data [12].

The current outcomes are found inconsistence with them with 0.1%-0.2% variations.

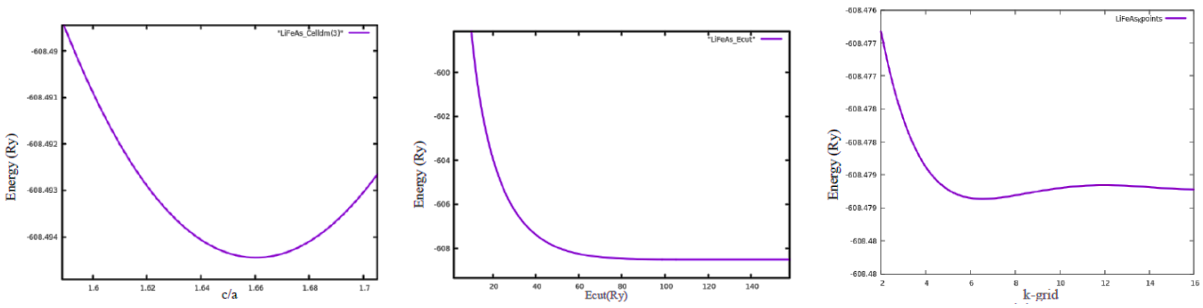

(a) (b) (c)

Figure 2: Optimization curves for (a) c/a, (b) E-cut, (c) k-grid for LiFeAs.

In this work, the gnuplot [43] in Figure 2 is used to plot the band structure for the given material. On the high symmetry points, Γ→ Z → R → X → M → A→ Γ, the k-points path in reciprocal space is taken into consideration. Here, the energy cutoff considered is 80 Ry, while the charge density cutoff is 320 Ry. In order to integrate over the Brillouin zone, a 6×6×6 k-pint mesh is used. Because Fe is ferromagnetic by nature, a spin component is introduced for the computations in both circumstances. In other words, plots of the band structures for up and down spin are available. From the band structure study, it is observed that, the LiFeAs has a metallic quality, as evidenced by the overlapping of band lines close to the Fermi region in Figure 2. Furthermore, no differences are seen between the situations of a minority and a majority. The Fermi energy (E_F) is found 9.6985 eV from the band structure data.

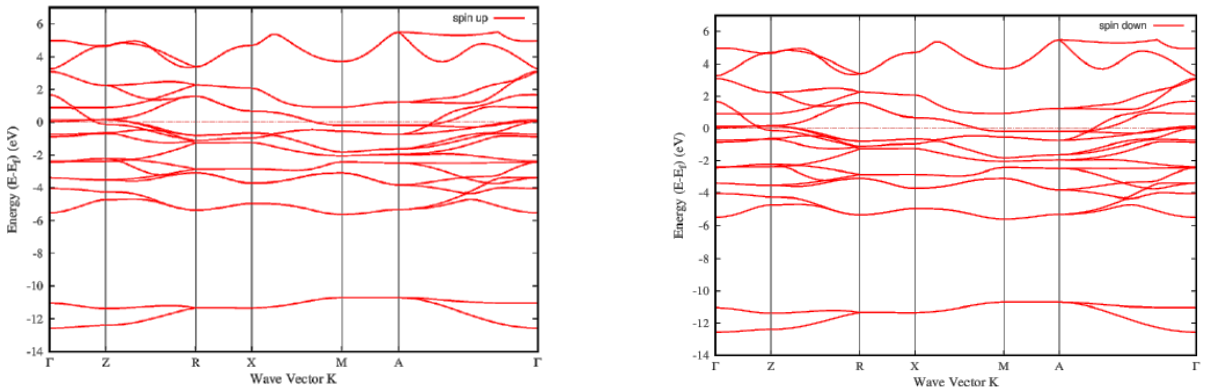

(a) (b)

Figure 3: Electronic band structure for LiFeAs (a) spin up (b) spin down.

Table 1: Calculated and experimental lattice parameters for LiFeAs.

Lattice Constants (Å)	**Presently Calculated Values**	**Experimental Values [?]**	**Deviation (%)**
a	3.790	3.791	0.1
c/a	1.6577	1.6599	0.2

The TDOS and PDOS for LiFeAs are displayed in Figures 3 and 4. In this case, the Fermi level electron density is seen at around 4.1 states/eV. At -10 eV, much below the E_F, an electron density of about 1.8 states/eV is also detected. Furthermore, there is no difference in the TDOS for spin-up and spin-down situations, which would point to its superconducting nature. It is evident from the partial DOS displayed in Figure 4 that the 3d state of Fe predominates close to the Fermi area. The 4s orbital of arsenic contributes significantly below the Fermi level. The density in the range of -5.0 eV to E_F clearly suggests that Fe and As are covalently bonded through hybridization between the Fe(3d)-As(3p) orbitals in Fe_2As_2 blocks. Consequently, the pnictogen bands and the 3d states of Fe are what give LiFeAs its metallic nature. From the Figure 3, the highest Fermi level DOS is observed around 4.2 states/eV.

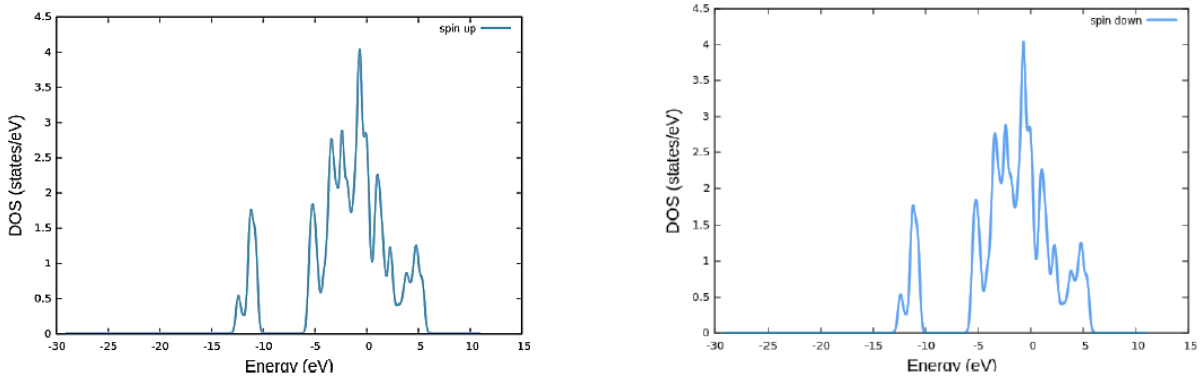

(a) (b)

Figure 4: TDOS of LiFeAs (a) spin up (b) spin down.

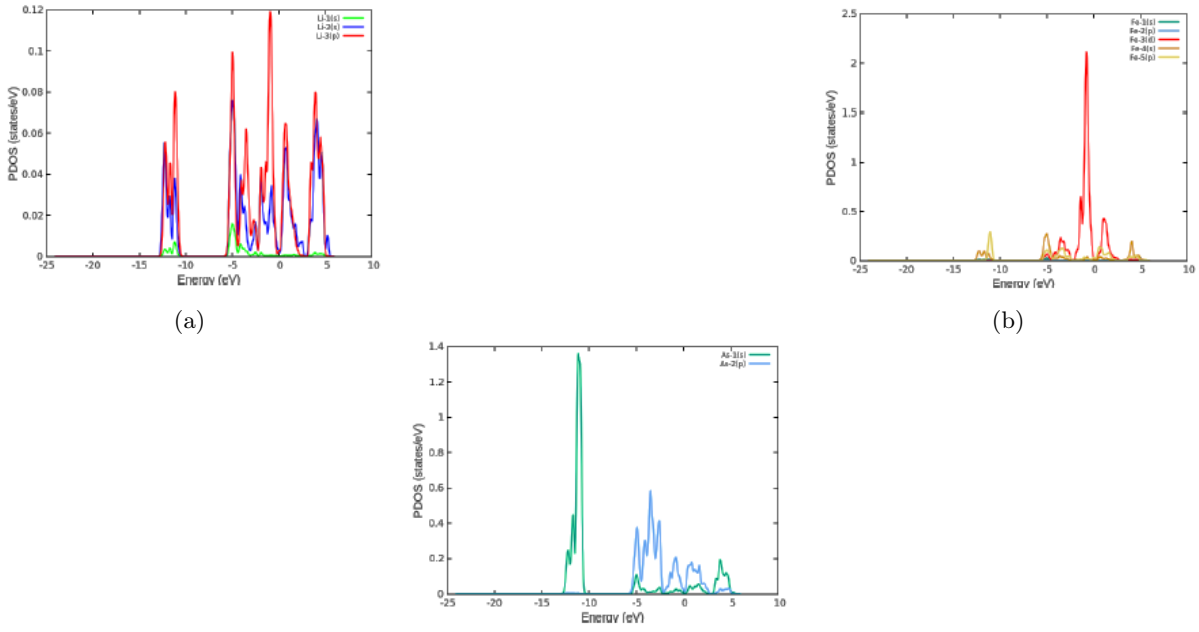

(a) (b)

(c)

Figure 5: PDOS of LiFeAs (a) Li, (b) Fe and (c) As.

In the present work, XCrySDen [44] software is used to analyze the Fermi surface topology of the material under investigation. The spin component is not included in the computation of the Fermi surface since there is no difference between the band structure and DOS for the spin-up and spin-down cases.

Five bands intersect the Fermi energy level E_F in the band structure of LiFeAs (Figure 2). These five bands are represented by their respective Fermi surfaces. They confirm that FeAs superconductors are often two-dimensional, as proposed by Sadovskii, Ivanovskii and Izyumov [2–4]. Figures 5(a)–(e) depict the Fermi surfaces for individual bands that pass through the E_F; Figures 5(f) and (g) show the Fermi surfaces for merged bands. The electron contribution is provided by the quasi-cylinders at the corners of the Brillouin zone in the M-A direction, while the hole-like concentric cylinders are located at the zone centre (). This way, the Fermi surfaces are visualized to discriminate between the occupied and unoccupied states. Hence, for the aforementioned materials, Fermi surfaces are created in a way that ascertains the electron contribution at the corners and the hole contribution in centre of the Brillouin zone.

The QE code's "PHonon" package is used to calculate phonons [40]. The energy cutoff of 80 Ry and the charge density cutoff of 320 Ry were taken into consideration while computing the phonon dispersion of studied material. It was assumed that the k-mesh was 6x6x6. The phonon dispersion was calculated over the high symmetry sites ($\Gamma \rightarrow Z \rightarrow R \rightarrow \Gamma$) of the Brillouin zone, taking into account the q-grid of $2 \times 2 \times 2$.

Due to their involvement in pairing interactions, electron and hole pockets in Fermi surface analysis have a major influence on superconductivity. By permitting interband scattering between electron and hole pockets, multiple pockets can improve superconductivity, particularly when spin or orbital fluctuations are involved. Unconventional $\pm$ wave pairing can be facilitated by mediating spin-density-wave-type fluctuations by nesting between electron pockets at the zone corners and hole pockets at the Brillouin zone center. The density of states at the Fermi level is influenced by the size and shape of pockets, with higher $N(E_F)$ typically strengthening pairing. The superconducting gap structure is influenced by electron-hole asymmetry; fully gapped states are preferred by balanced pockets, whereas nodes or anisotropic gaps may result from severe imbalance. The momentum-space "playground" for pairing interactions is defined by Lifshitz transitions, which can result in abrupt changes in T_c.

The phonon DOS and phonon dispersion curves for LiFeAs are shown in Figure 6. The dispersion curve has 18 phonon branches, including 2 TA, 1 LA, 5 LO, and 10 TO mode branches. A phonon dispersion of 0 cm^{-1} to 695 cm^{-1} is computed. The LiFeAs crystal structure's dynamical stability is suggested by the positive phonon frequencies. The appropriately degenerate states of different optical and acoustical branches at point R are visible at 100 cm^{-1}, 125 cm^{-1}, 190 cm^{-1}, 255 cm^{-1}, 275 cm^{-1}, 295 cm^{-1}, 510 cm^{-1}, and 580 cm^{-1}. Additionally, an overlapping of the acoustical and optical branches is visible at 125 cm^{-1}. It is discovered that the highest phonon branches are very dispersive in the Z-R direction. Because of the overlapped, weakly dispersive optical branches, the phonon DOS about 290 cm^{-1} has its maximum peak. There is a little band gap seen around 210 cm^{-1}. Certain peaks are identified in the phonon DOS at 100 cm^{-1}, 120 cm^{-1}, 15 cm^{-1}, 210 cm^{-1}, 230 cm^{-1}, 290 cm^{-1}, 300 cm^{-1}, and 315 cm^{-1}. From the Figure 6 it is observed that, the highest phonon frequency noted around at 698 cm^{-1} at R point.

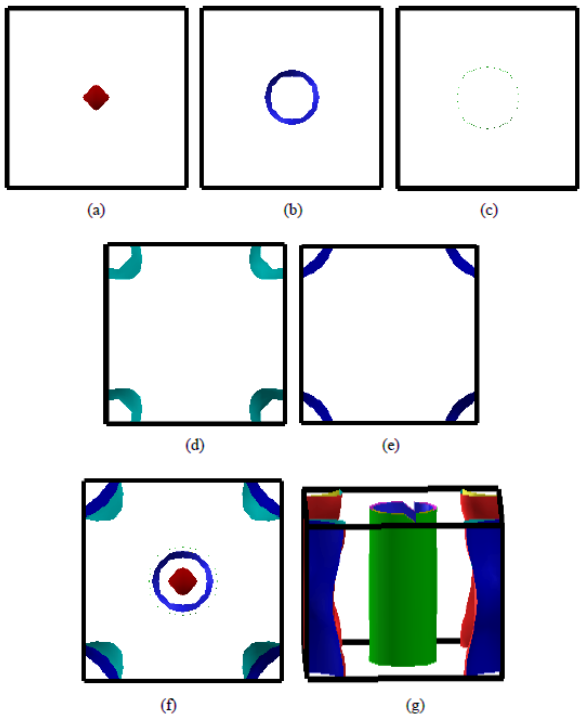

Figure 6: The Fermi surfaces for different bands (a)-(e) and for merged bands (f) and (g).

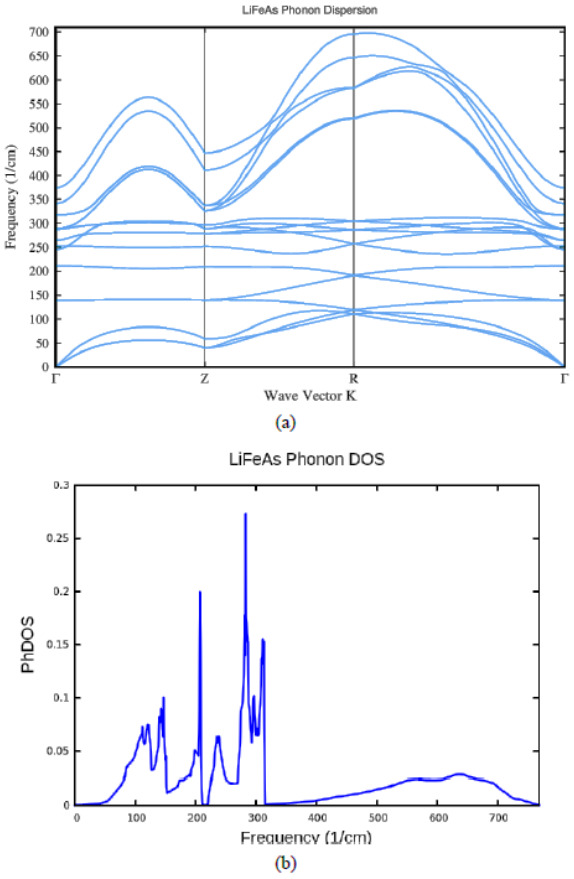

Figure 7: (a) Phonon dispersion curve and (b) phonon DOS.

4 Conclusions

Ultimately, we draw the conclusion that the structural, electronic and vibrational properties of

LiFeAs, an iron pnictide superconductor are reported in the present paper. It is observed that 3s state of 'As' predominates in the section far below the Fermi level and that the 3d states of 'Fe' and 'Li' are found near to and above the Fermi level, respectively. The metallic character of LiFeAs is demonstrated by the superimposing bands near to the Fermi level. Furthermore, dynamic stability of aforementioned structure is suggested by the positive frequencies in the phonon dispersion curves.

The author expresses heartfelt gratitude to the Department of Science and Technology, Government of India, New Delhi, India, for developing the computing facility under the DST-FIST program and to the University Grants Commission, New Delhi, India, for providing financial support under the DRS-SAP-II program.

Conflict of interest

There was no disclosed conflict of interest by the author(s).

References

[1] Y. Kamihara, T. Watanabe, M. Hirano, and H. Hosono. Iron-based layered superconductor la[$O_{1-x}f_x$]FeAs (x = 0.05–0.12) with t_c = 26 k.

[2] M. V. Sadovskii. High-temperature superconductivity in iron-based layered iron compounds. *Physics-Uspekhi*, 51:1201–1227, 2008.

[3] A. L. Ivanovskii. New high-temperature superconductors based on rare earth and transition metal oxyarsenides and related phases: synthesis, properties and simulation. *Physics-Uspekhi*, 51:1229–1260, 2008.

[4] Y. A. Izyumov and E. Z. Kurmaev. Feas systems: a new class of high-temperature superconductors. *Physics-Uspekhi*, 51:1261–1286, 2008.

[5] H. Hosono. Iron pnictide superconductors: Discovery and current status. *Materials Matters*, 4:1–11, 2011.

[6] H. Hosono, K. Tanabe, E. Takayama-Muromachi, H. Kageyama, S. Yamanaka, H. Kumakura, M. Nohara, H. Hiramatsu, and S. Fujitsu. Exploration of new superconductors and functional materials, and fabrication of superconducting tapes and wires of iron pnictides. *Science and Technology of Advanced Materials*, 16:033503, 2015.

[7] Qimiao Si, Rong Yu, and Elihu Abrahams. High-temperature superconductivity in iron pnictides and chalcogenides. *Nature Reviews Materials*, 1:16017, 2016.

[8] R. M. Fernandes, A. I. Coldea, H. Ding, I. R. Fisher, P. J. Hirschfeld, and G. Kotliar. Iron pnictides and chalcogenides: a new paradigm for superconductivity. *Nature*, 601:35–44, 2022.

[9] S. A. Rasaki, T. Thomas, and M. Yang. Iron based chalcogenide and pnictide superconductors: From discovery to chemical ways forward. *Progress in Solid State Chemistry*, 59:100282, 2020.

[10] H.-H. Wen and S. Li. Materials and novel superconductivity in iron pnictide superconductors. *Annual Review of Condensed Matter Physics*, 2:121–140, 2011.

[11] X. C. Wang, Q. Liu, Y. X. Lv, W. B. Gao, L. X. Yang, R. C. Yu, F. Y. Li, and C. Q. Jin. The superconductivity at 18 k in lifeas system. *Solid State Communications*, 148:538–540, 2008.

[12] J. H. Tapp, Z. Tang, B. Lv, K. Sasmal, B. Lorenz, P. C. W. Chu, and A. M. Guloy. Lifeas: An intrinsic feas-based superconductor with $t_c = 18$ k. *Physical Review B*, 78:060505, 2008.

[13] M. M. Qazilbash, J. J. Hamlin, R. E. Baumbach, L. Zhang, D. J. Singh, M. B. Maple, and D. N. Basov. Electronic correlations in the iron pnictides. *Nature Physics*, 5:647–650, 2009.

[14] E. Bascones, B. Valenzuela, and M. J. Calderón. Magnetic interactions in iron superconductors: A review. *Comptes Rendus Physique*, 17:36–59, 2016.

[15] F. Mancini and R. Citro, editors. *The Iron Pnictide Superconductors: An Introduction and Overview*, volume 186 of *Springer Series in Solid-State Sciences*. Springer, 2017.

[16] S. L. Drechsler, H. Rosner, M. Grobosch, G. Behr, F. Roth, G. Fuchs, K. Koepernik, R. Schuster, J. Malek, S. Elgazzar, M. Rotter, D. Johrendt, H. Klauss, B. Büchner, and M. Knupfer. New insight into the physics of iron pnictides from optical and penetration depth data. arXiv preprint arXiv:0904.0827v1 [cond-mat.supr-con], 2009.

[17] K. Motizuki, T. Itoh, H. Ido, and M. Morifuji. Electronic structure and magnetism of 3d-transition metal pnictides. In R. Hull, C. Jagadish, R. M. Jr. Osgood, J. Parisi, Z. Wang, and H. Warlimont, editors, *Springer Series in Materials Science*. Springer, 2009.

[18] H. Hosono, A. Yamamoto, H. Hiramatsu, and Y. Ma. Recent advances in iron-based superconductors toward applications. *Materials Today*, 21:278–302, 2018.

[19] D. S. Inosov. Spin fluctuations in iron pnictides and chalcogenides: From antiferromagnetism to superconductivity. *Comptes Rendus Physique*, 17:60–89, 2016.

[20] K. Ishida, Y. Nakai, and H. Hosono. To what extent iron-pnictide new superconductors have been clarified: A progress report. *Journal of the Physical Society of Japan*, 78:062001, 2009.

[21] M. Johannes. The iron age of superconductivity. *Physics*, 1:28, 2008.

[22] D. S. Inosov. Spin fluctuations in iron pnictides and chalcogenides: From antiferromagnetism to superconductivity. *Comptes Rendus Physique*, 17:60–89, 2016.

[23] K. V. Mitsen and O. M. Ivanenko. Cluster structure of superconducting phase and the nature of peaks in the doping dependences of the london penetration depth in iron pnictides. *Results in Physics*, 32:105156, 2022.

[24] S. V. Borisenko, V. B. Zabolotnyy, D. V. Evtushinsky, T. K. Kim, I. V. Morozov, A. N. Yaresko, A. A. Kordyuk, G. Behr, A. Vasiliev, R. Follath, and B. Büchner. Superconductivity without nesting in lifeas. *Physical Review Letters*, 105:067002, 2010.

[25] V. B. Zala, A. M. Vora, and P. N. Gajjar. Electronic properties of iron pnictide superconductor lifep. In *AIP Conference Proceedings*, volume 2100, page 020027, 2019.

[26] I. R. Shein and A. L. Ivanovskii. Electronic properties of novel 6 k superconductor lifep in comparison with lifeas from first principles calculations. *Solid State Communications*, 150:152–156, 2010.

[27] S. J. Zhang, X. Wang, R. Sammynaiken, J. Tse, L. Yang, Z. Li, Q. Liu, and C. Jin. Effect of pressure on the iron arsenide superconductor lixfeas (x = 0.8, 1.0, 1.1). *Physical Review B*, 80:014506, 2009.

[28] Y. Mizuguchi, F. Tomioka, S. Tsuda, T. Yamaguchi, and Y. Takano. Superconductivity at 27 k in tetragonal fese under high pressure. *Applied Physics Letters*, 93:152505, 2008.

[29] Materials Project. Lifeas (mp-21471). https://next-gen.materialsproject.org/materials/mp-21471?formula=LiFeAs. Accessed: 2025-08-16.

[30] V. B. Parmar and A. M. Vora. Study of structural and electronic properties of intercalated transition metal dichalcogenides compound mtis2 (m = cr, mn, fe) by density functional theory. *East European Journal of Physics*, 1:93–98, 2021.

[31] V. B. Parmar and A. M. Vora. Study of structural and electronic properties of intercalated crtis2 compound by density functional theory. *Eurasian Journal of Physics and Functional Materials*, 5:116–125, 2021.

[32] H. S. Patel, V. A. Dabhi, and A. M. Vora. To study the structural and electronic properties of tibeo3 using density functional theory. In D. Singh, S. Das, and A. Materny, editors,

Advances in Spectroscopy: Molecules to Materials, volume 236 of *Springer Proceedings in Physics*, pages 389–395. Springer, 2019.

[33] V. A. Dabhi, H. S. Patel, and A. M. Vora. To investigate electronic properties of alho2 doped with trivalent impurities (ga, in, tl) by using density functional theory. In *AIP Conference Proceedings*, volume 2224, page 030003, 2020.

[34] H. S. Patel, V. A. Dabhi, and A. M. Vora. Elastic constants of beryllium oxide: A first-principles investigation. In *AIP Conference Proceedings*, volume 2224, page 030006, 2020.

[35] V. A. Khalas, V. B. Parmar, and A. M. Vora. A density functional theory based study of transition metal dichalcogenide-mos2. *Materials Today: Proceedings*, 67:165–169, 2022.

[36] H. S. Patel, V. A. Dabhi, and A. M. Vora. Adverse effect of k-mesh shifting in several crystal systems: An analytical study. *Materials Today: Proceedings*, 57:275–278, 2022.

[37] V. A. Dabhi, H. S. Patel, and A. M. Vora. Investigation of thermoelectric properties of galena using density functional theory. *Materials Today: Proceedings*, 67:137–140, 2022.

[38] H. S. Patel, V. A. Dabhi, and A. M. Vora. First principles investigation of thermoelectric properties of tibeo3. *Materials Today: Proceedings*, 67:151–155, 2022.

[39] V. B. Parmar and A. M. Vora. Study of structural and electronic properties of mntis2 compound. *Sri Lankan Journal of Physics*, 23:16–25, 2022.

[40] P. Giannozzi, S. Baroni, N. Bonini, M. Calandra, R. Car, C. Cavazzoni, D. Ceresoli, G. Chiarotti, M. Cococcioni, I. Dabo, and A. Dal Corso. Quantum espresso: a modular and open-source software project for quantum simulations of materials. *J. Phys. Condens. Matter*, 21:395502, 2009.

[41] J. P. Perdew, K. Burke, and M. Ernzerhof. Generalized gradient approximation made simple. *Phys. Rev. Lett.*, 77:3865–68, 1996.

[42] D. Vanderbilt. Soft self-consistent pseudopotentials in a generalized eigenvalue formalism. *Phys. Rev. B*, 41:7892–7895, 1990.

[43] P. K. Janert. *Gnuplot in Action: Understanding Data with Graphs*. Manning Publications, Greenwich, CT, 2009.

[44] A. Kokalj. Xcrysden—a new program for displaying crystalline structures and electron densities. *J. Mol. Graph. Model.*, 17:176–179, 1999.